Tunable superradiance in porphyrin chains on insulating surfaces

Tunable superradiance in porphyrin chains on insulating surfaces

S M Vlaming and A Eisfeld

Max Planck Institute for the Physics of Complex Systems, Nöthnitzer Strasse 38, D-01187 Dresden, Germany

E-mail: vlaming@pks.mpg.de

Abstract

Recent experiments have shown that it is possible to synthesize collections of one-dimensional chains of non-covalently bound porphyrins on various surfaces. We provide a study of the optical properties of these systems, and we show that generally one expects the appearance of multiple superradiant transitions, which can be both redshifted or blueshifted with respect to the monomer transitions. Moreover, porphyrin chains can simultaneously support both redshifted and blueshifted features in the absorption spectrum. The energies, absorption strengths and polarizations of the excitonic transitions can be understood in terms of Davydov splitting of chains with one transition per molecule. A distribution over chain lengths and energy relaxation due to coupling to the environment are proposed as mechanisms for the broadening of the superradiant transitions.

Keywords: porphyrin nanostructures, superradiance, Frenkel excitons, optoelectronics

(Some figures may appear in colour only in the online journal)

1. Introduction

The creation of molecule-based nanostructures on surfaces is of great interest from the point of view of molecular electronics. In the bottom-up approach, the techniques of supramolecular chemistry are used to produce tailored structures with specific functional properties [1–3]. By modifying the monomer species, side groups and the substrate properties, it is possible to modify the non-covalent interactions between the molecular building blocks, and thereby influence the self-assembly process. This allows for a variety of geometries that have been created over the years. In addition, different substrates may be used depending on the intended application, and a wide range of molecule-based structures have been synthesized on metallic, semiconductor as well as insulating substrates [4–6]. If one intends to decouple the supramolecular nanostructure as much as possible from the substrate, the latter option is most desirable [7, 8].

The close proximity of the non-covalently bound porphyrins in these structures imply intermolecular resonance interactions, suggesting a collective optical response and coherent excitations. A proper understanding of the nature of the collective electronic excitations and spectroscopical properties is important in the view of possible optoelectronic applications. Recent experiments on the semiconductor 3,4,9,10-perylenetetracarboxylic acid dianhydride (PTCDA) on dielectric surfaces [8] have shown that one is, on the one hand, able to obtain high resolution optical spectra of both single molecules and supramolecular structures. On the other hand, the supramolecular structure leads to a coherent collective excitation of many molecules [9, 10]. The collective nature of the excitations leads to a reduced coupling to vibrational modes and a strong reduction of the radiative emission lifetime, a phenomenon known as superradiance. In turn, superradiance also affects the absorption spectra, typically leading to shifted and narrowed absorption features [10, 11].

Porphyrins (and related molecules such as phthalocyanines, chlorophylls, and hemes) [12–14] provide excellent candidates for the use in molecular wires or photosynthetic antennae. There is a wide variety of synthetically available porphyrin derivatives with different side groups and coordination complexes, allowing for the tailoring of the monomer species to enhance the aggregation process and to modify the physical properties of the nanostructure [5, 15]. Moreover, they are chemically stable, cheap, and have highly desirable optical and energy transport properties due to their

large transition dipoles in and around the visible spectrum. A range of structures based on porphyrins have previously been synthesized and studied, such as covalently coupled wires [16–19], porphyrin aggregates [15, 20–24] and various porphyrin arrays on surfaces [25–29].

Recent studies have shown the creation of non-covalently bound, effectively one-dimensional porphyrin structures on insulating substrates. Meyer and co-workers [30–32] have synthesized chains of tilted porphyrins, both on monolayers and along step edges. In particular, cyanoporphyrins have been shown to form nanowires (among other observed geometries) on a KBr(0 0 1) substrate [30, 31], preferably along the straight step edges. The porphyrins are tilted with respect to the surface and stabilized by electrostatic interactions of the side groups with the surface, with π–π stacking between the porphyrin rings. Likewise, in [33], it is reported that the deposition of a thin CoO layer onto an Ir(1 0 0) surface creates a one-dimensional Moiré pattern. These regularly spaced distortions lead to a preferential attachment of the porphyrins onto these spots, essentially enabling the formation of one-dimensional porphyrin nanostructures. The molecules lie flat on the surface here, and various relative orientations are possible [34]. Likewise, a flat stacking of porphyrins on the substrate has been observed for various other substrate materials [5, 35].

The emphasis in [30, 31, 36] has been on the synthesis and characterization through noncontact atomic force microscopy (nc-AFM) of the wires. In this paper, we provide a predictive study of the optical properties of one-dimensional porphyrin wires. In contrast to the PTCDA case where each molecule has only one optical transition of relevance [8], porphyrins may have multiple optical transitions that allow for nontrivial geometrical possibilities and interesting collective excitonic effects. In this paper, we will provide a general treatment that can be applied to chains of similar molecules, as long as there are two perpendicularly polarized transitions present in the monomer. The theoretical framework here can easily be extended to other molecules with multiple molecular transitions. Likewise, the approach presented here may apply to other substrates and also one-dimensional covalently bound porphyrin structures, as long as neither the substrate nor the covalent bond significantly distort the optically relevant monomeric electronic wave functions. In a more specific example, we will provide predictions for the optical properties of experimentally realized porphyrin wires, similar to those reported in [30, 31, 36] and those which can be realized in the system of [33]. In particular, we show that interesting collective optical behaviour exists in these systems: we predict the occurrence of superradiance, and in fact the porphyrin wires will typically support a double peaked absorption spectrum where both peaks are shifted away from the monomer absorption peak. A distribution over chain lengths will lead to additional peaks, and we suggest the possibility of a finite size induced broadening of the absorption peaks, in addition to the thermal broadening caused by coupling to the environment.

In section 2, we introduce the theoretical background necessary to calculate the optical properties of the systems mentioned above. First, we provide a general description on the occurrence of exciton states and their absorption properties in section 2.1. In section 2.2, we show some analytical results that facilitate the understanding of the expected optical properties of porphyrin chains. We then proceed with numerical simulations of the absorption properties of various experimentally feasible porphyrin chain conformations in section 3. Specifically, in section 3.1 we first focus on the absorption of chains of porphyrins that lie flat on the surface, and how this depends on the various parameters and the relative orientation of the porphyrin molecules. In section 3.2, the discussion is generalized to chains of tilted porphyrins, i.e. as in [30, 31, 36]. We conclude in section 4.

2. Theoretical considerations

The optical response of monomeric phthalocyanines and porphyrins is typically dominated by two bands of transitions in the (near) visible part of the spectrum [12–14]. At low energies (around 1.5–2 eV, typically) there is the so-called Q-band, consisting of two transitions that are polarized perpendicularly to each other and are referred to as the Q_x and Q_y transitions. These are often strongly coupled to vibrational modes of the molecule, leading to additional vibronic sidepeaks (at higher energies). In addition, there are two perpendicular transitions (labelled B_x and B_y) at considerably higher energies, forming the Soret band at transition frequencies in the near ultraviolet (around 2.5–3 eV). The two B or Q-transitions may be degenerate but are not necessarily so, depending on the symmetry, the side groups and the environment. The transition dipoles are likewise not necessarily equal in magnitude due to symmetry breaking considerations (e.g., the Q transition is only weakly allowed in porphins due to symmetry [37]). The Soret band transitions tend to be stronger, with transition dipole moments that can easily reach $\mu = 10$–13 D, while the Q transitions are typically found to be weaker, with transition dipole moments of the order of $\mu = 3$–7 D found for various porphyrin derivatives, see e.g. [17, 24, 38, 39, 40]. Specifically, the Q band transition dipole magnitude of the cyanoporphyrin derivatives used by the Meyer group is estimated at $\mu \approx 4.4$ D [30]. There may be additional weak transitions, referred to as N and Tx1–Tx3 transitions; we will not concern ourselves with those in this paper since it will not add to the qualitative predictions presented here.

For clarity's sake, we will treat the two optically dominant bands separately. A treatment of these four electronic excitations (B_x, B_y, Q_x and Q_y) simultaneously is straightforwardly implemented in the formalism presented here. However, while it is known that coupling between the two bands may lead to some intensity borrowing and additional shifts, it does not lead to any qualitative alterations in the predictions we make here. For a study of the effect of coupling between the B and Q-transitions in three related systems, namely β-tetraethylpyridinylporphyrin aggregates [41], chlorophylls/bacteriochlorophylls [42, 43], and tetra(4-sulphonatophenyl)porphyrin nanotubes [44], we refer to [41–44]. In addition, we focus our study on porphyrin-based structures on insulating substrates. Here, the coupling between the molecules and the substrate is weak [7], and the optical

J. Phys. D: Appl. Phys. **47** (2014) 305301

S M Vlaming and A Eisfeld

response of the porphyrin structures is well captured by a tight-binding model where interactions with the substrate are neglected.

2.1. General formalism

We consider a chain consisting of N non-covalently bound porphyrin molecules, where each molecule is allowed to have multiple optically relevant transitions, which we label by j. Each such transition has an associated transition dipole moment $\vec{\mu}_j$, which couples the electronic transitions to the electric field of the incoming light, and in addition induces an interaction between the various molecular transitions. This interaction leads to excitations that will be coherently shared over (part of) the chain. We label the molecules in the chain by n, and the transitions within a porphyrin by j. The corresponding Frenkel exciton Hamiltonian is [45, 46]

$$H = \sum_{nj} \omega_{nj} \, |n; j\rangle \langle n; j| + \sum_{njn'j'} J_{jj'} (n-m) \, |n; j\rangle \langle m; j'| ,$$

(1)

where $|n; j\rangle$ is the state where molecule n has the j-th transition excited, while all others are in the ground state, and ω_{nj} is its corresponding transition energy. The interaction $J_{jj'}(n-m)$ between transition j on molecule n and transition j' on molecule $m \neq n$ is mediated through their transition dipole moments. Typically, we will use point dipole or extended dipole interactions here, although the formalism allows for more general expressions for the interactions as well. Note that a similar formalism may be applied to covalently bound porphyrin wires, as long as the covalent bonding does not disturb the relevant electronic wave functions of the porphyrins to a significant extent. In addition, while we focus on porphyrins in this paper, the formalism here can be applied to other molecules with multiple relevant molecular transitions j as well.

The relevant collective excited states (excitons) that will be optically excited are the eigenstates of equation (1), which we can write as

$$|q\rangle = \sum_{n,j} c_{qnj} \, |n; j\rangle ,$$

(2)

with corresponding eigenenergy E_q. There are N times j such exciton states, forming a band around the monomer transition energy with a bandwidth proportional to the exchange interaction strength.

The linear absorption spectrum is an easily accessible experimental quantity that allows us to probe the collective, superradiant nature of the electronic excited states [45, 46]. The molecules couple to incoming light, and in particular to the electric field of the incoming light, through their transition dipole moments. Commonly, one considers the coupling of the transition dipole moments of the molecules and the electric field of the light as a perturbation to the Hamiltonian equation (1), and uses the Fermi golden rule. The effective transition dipole moment of the exciton state q is $\vec{\mu}_q = \sum_{n,j} c_{qnj} \vec{\mu}_{nj}$, which leads to an absorption strength of

$$O_q = \left| \vec{\mu}_q \cdot \vec{e} \right|^2 ,$$

(3)

where $\vec{e}$ is the polarization vector of the incoming light. The absorption strength O_q is a measure of how strongly the transition from the electronic ground state to the excited state q couples to the incoming light, and corresponds to the area of the absorption peak at energy E_q, so that the linear absorption spectrum is given by

$$A(\omega) = \sum_q O_q \delta \left(E_q - \omega \right) .$$

(4)

Generally, while there are Nj states, only a few states absorb strongly: these are the superradiant states where the molecules absorb in phase. Note that we will use the term superradiance for any collective state with a strongly enhanced absorption strength, and thereby a strongly enhanced absorption and emission rate. The state in question need not necessarily feature prominently in the emission spectrum, due to possible ultrashort lifetimes as a result of relaxation processes. The linear absorption spectrum will be dominated by the absorption into the superradiant states. For (predominantly) negative interactions, the superradiant state occurs at the bottom of the band, at an energy below the monomer transition, giving the so-called J-band absorption peak. For positive interactions, the state that is superradiant is at the top of the band, i.e. at a higher energy than the monomer transition—this is referred to as an H-band. Interestingly enough, as we will see in section 3, one-dimensional porphyrin chains can exhibit both these features at the same time.

To obtain an absorption lineshape, we employ the formalism developed in [47]. Here, we assume that the electronic transitions couple weakly to acoustic phonon modes, allowing for relaxation to lower lying exciton states. The corresponding dephasing leads to a thermal broadening effect. We refer to [47] for a detailed discussion; in addition, the relevant expressions have been included in appendix D. We do not include coupling of the electronic transitions to the vibrational modes of the porphyrin (e.g. vibronic progressions), as this goes beyond the scope of the present work. Within this approach, one includes exciton dephasing rates Γ_q, and the absorption is given by

$$A(\omega) = \sum_q \frac{O_q}{\pi} \frac{\Gamma_q}{\left(\omega - E_q \right)^2 + \Gamma_q^2} .$$

(5)

The local environment of the porphyrin monomers changes from molecule to molecule, and the inhomogeneities resulting from such local interactions lead to disorder in the monomer properties. Such disorder is known to lead to localization of the exciton wave functions [48, 49]. However, since the experimental systems that we are interested in typically consist of mostly short chains, i.e. shorter than the localization length, finite size effects dominate over localization effects [50]. Therefore, we can treat the systems as being homogeneous to an excellent approximation. Numerical calculations indeed confirm that the results presented in this paper do not change appreciably upon the inclusion of realistic amounts of disorder. In the following, we ignore disorder, and coupling to internal and external vibrations is only included as a thermal broadening mechanism, as discussed above.
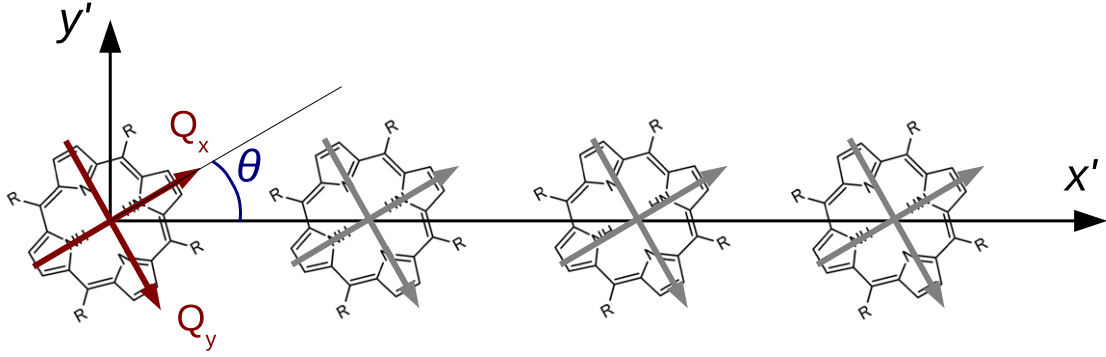
Figure 1. Geometry of flat-lying porphyrins on a surface. The direction of the transition dipole moments of the Q_x and Q_y transitions of the first molecule are denoted by the red arrows. All other porphyrins are oriented in the same way, with their transition dipole moment orientations denoted by grey arrows. The geometry is fully fixed by the interporphyrin distance a and the angle θ between the transition dipole moment of the Q_x transition and the horizontal x'-axis.

2.2. Non-disordered porphyrin chains

Upon defining the interactions and energies in equation (1), the framework provided in section 2.1 already allows for a direct, brute force numerical calculation of the optical properties of the porphyrin chains under consideration. However, it is insightful to first consider the non-disordered case (i.e., $\omega_{nj} = \omega_j$ in equation (1)) in more detail. We will focus on the main results here, leaving the details to appendix A.

In the absence of disorder, we can partially diagonalize the Hamiltonian equation (1) by applying the transformation $|k\rangle = \sum_n c_{kn}|n\rangle$ $(k = 1...N)$ that would diagonalize a chain with one transition per molecule [24, 45],

$$H = \sum_k \left(\sum_{jj'} \omega_{k,jj'} |kj\rangle \langle kj'| \right) \equiv \sum_k H(k). \quad (6)$$

The partial diagonalization then leads to a set of $j \times j$-Hamiltonians that remains to be diagonalized. We denote the exciton coefficients of this remaining diagonalization by d_{sj}.

The full diagonalization can then be written as

$$|k; s\rangle = \sum_{nj} c_{kn} d_{sj} |n; j\rangle, \quad (7)$$

and we can calculate the effective transition dipole moment of the exciton state (k, s) through

$$\vec{\mu}_{ks} = \sum_{nj} c_{kn} d_{sj} \vec{\mu}_{nj}. \quad (8)$$

As detailed in appendix A, only a few values of k give significant contributions to the absorption spectrum. More specifically, the absorption spectrum is dominated by the values of k corresponding to superradiant states, in particular $k = 1$, where the various molecules absorb in phase. The existence of off-diagonal contributions in the corresponding $j \times j$-Hamiltonian $H(k)$ leads to an additional Davydov splitting and a redistribution of absorption strength over the j peaks [24, 45]. The important point here is that the physics of the full system can be understood as a $j \times j$-Hamiltonian, where each element corresponds to a Hamiltonian contribution

for one transition per molecule. In addition, the dominant contribution to the absorption spectrum is given by the $j \times j$-Hamiltonian for the superradiant transition $k = 1$. Finally, note that the exciton energies and absorption strengths, as given in appendix A, have a dependence on the chain length N. This is particularly pertinent since, in experiment, the chains are typically fairly short (i.e. where that the length dependence is strongest), and some distribution over chain lengths will occur.

3. Absorption of porphyrin chains

We now proceed with the numerical calculation of typical absorption spectra that are to be expected in various experimental situations. Firstly, we need to define the geometry of the system, in particular the relative positions and orientations of the porphyrins. We consider both systems where the porphyrins are lying flat on the surface [33], and in addition, we consider chains of tilted porphyrins [30–32]. As detailed in appendix B, we can show analytically that for flat-lying porphyrins with degenerate transitions, the absorption spectrum is independent of the orientation.

After defining the geometry by specifying the molecular positions, the magnitude and orientation of the corresponding transition dipole moments, and the transition energies, the absorption spectrum is straightforwardly calculated by the methods in section 2.1. We focus on the Q-band here, since these are the lowest energy electronic excited states and therefore have a relatively long lifetime. A similar analysis can be made for the Soret band, but here one should keep in mind that fast decay and relaxation processes can occur. Without loss of generality, we define the x'-axis as connecting the centres of the molecules (each a distance a apart) and the y'-axis perpendicular to it, and we denote the angle that the Q_x transition dipole moment vector makes with the x'-axis by θ, as also shown in figure 1. Since the Q_y transition has its dipole moment oriented perpendicular to the Q_x transition, θ fully defines the in-plane geometry. Explicitly, we have $\vec{\mu}_x = \mu_x(\cos\theta, \sin\theta, 0)$ and $\vec{\mu}_y = \mu_y(\sin\theta, -\cos\theta, 0)$. To construct a tilted geometry, we require two additional angles α and β, as defined in appendix C.

As mentioned in section 2.1, and detailed in appendix D, we include thermal broadening of the exciton states to obtain
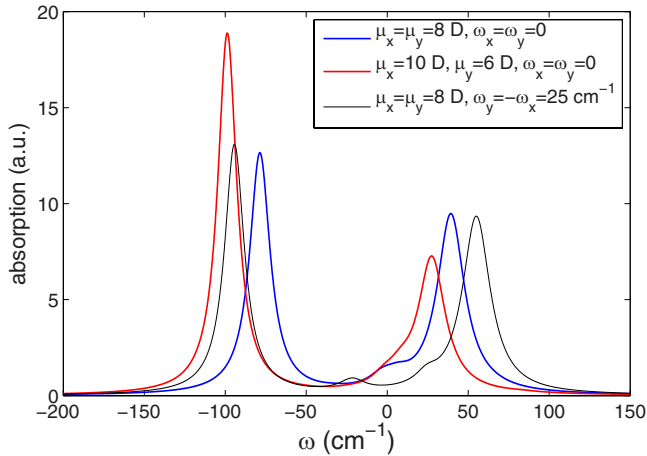
Figure 2. Three typical absorption spectra for a porphyrin chain of length $N = 5$, for several combinations of parameters: equipotent and degenerate transitions (blue line), degenerate transitions of different strength (red), equipotent and non-degenerate transitions (black). All shown spectra are for $\theta = 30°$. For all parameters, the spectrum is dominated by two peaks.

a lineshape. Specifically, we perform the calculations at approximately room temperature, $k_B T = 200 \, \text{cm}^{-1} \hat{=} 286 \, \text{K}$, and we choose a linear spectral density with a prefactor $W_0 = 0.05$.

3.1. In-plane porphyrins

In this section, we show some typical absorption spectra for realistic parameters. Here, we consider porphyrin chains that lie flat on the surface; given the physical size of a typical porphyrin, we take a lattice parameter of $a = 2.5 \, \text{nm}$. We express all transition frequencies with respect to a reference energy $\omega_0 = (\omega_x + \omega_y)/2$, i.e. in the plots in figure 2 to figure 6 the frequency ω is relative to ω_0. For degenerate transitions, this implies that $\omega_x = \omega_y = \omega_0 \hat{=} 0$. We take transition dipole moments of the order of $\mu_x = \mu_y = 8 \, \text{D}$, which is the correct order of magnitude for porphyrins [22, 24, 38], as also discussed in section 2. Generally, the shifts calculated here will be proportional to μ^2, as shown below as well as in appendix A. Therefore, the shifts and the corresponding energy splitting will be more pronounced for Soret band transitions than for Q band transitions. For the flat-lying porphyrins, the orientation is fully defined by the angle θ between the Q_x transition and the x'-axis, the latter being in the direction of the vector connecting the porphyrins (see figure 1). In the simulations in figure 2 to figure 4, we consider chains of length $N = 5$, while we discuss the length dependence and distributions over the chain lengths in figure 5.

A few typical absorption spectra are shown in figure 2. The absorption spectrum is generically dominated by two main peaks. These correspond to the eigenstates of the 2×2 Hamiltonian matrix for the superradiant k-state; the absorption strength of the two superradiant states of the uncoupled system is redistributed over the two new eigenstates. This typically leads to a redshifted J-peak, and a blueshifted H-peak. For typical parameters corresponding to flat-lying porphyrins, the interactions and energy spacings between the excitonic levels
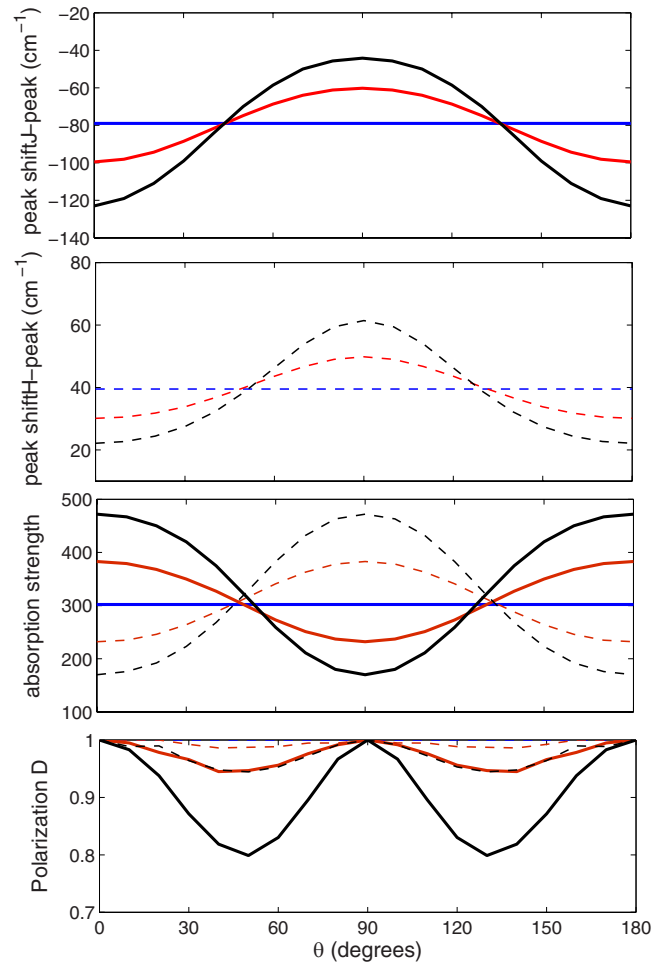
Figure 3. Peak position (upper two graphs), absorption strength (third graph) and polarization (bottom graph) of the two main superradiant peaks as a function of the orientation angle θ, for degenerate transitions. Thick lines: J-transition, thin dashed lines: H-transition. All curves are for degenerate transitions. The blue curve corresponds to equally strong transitions $\mu_x = \mu_y = 8 \, \text{D}$, the red curve is for $\mu_x = 9 \, \text{D}$, $\mu_y = 7 \, \text{D}$, and black is for $\mu_x = 10 \, \text{D}$, $\mu_y = 6 \, \text{D}$. For the first case (blue lines), there is no orientational dependence; in the more general case, the peak positions and absorption strengths vary $\propto \cos(2\theta)$ between the two extremes.

are of the order of tens up to a few hundred cm^{-1}. Again, energy splitting magnitudes for superradiance in the Q band transitions tend to be on the lower end of this range, while the energy splitting is larger for Soret band transitions. Either way, the typical energy spacings are small compared to the thermal energy $k_B T = 200 \, \text{cm}^{-1}$, and it becomes apparent that all states have a comparable dephasing rate and correspondingly, a comparable linewidth. This is clearly visible in figure 2, where the two peaks have similar widths. To succinctly summarize the dependence of the absorption spectra on changes in the various parameters, we show plots such as figure 3 and figure 4. In figure 3 and figure 4, we show how the peak position (i.e., the transition energy of the superradiant peaks), the absorption strengths and the polarization of these peaks depend on the orientation angle θ. Figure 3 shows results for degenerate transitions with different transition dipole moments, while figure 4 does the same for non-degenerate transitions with
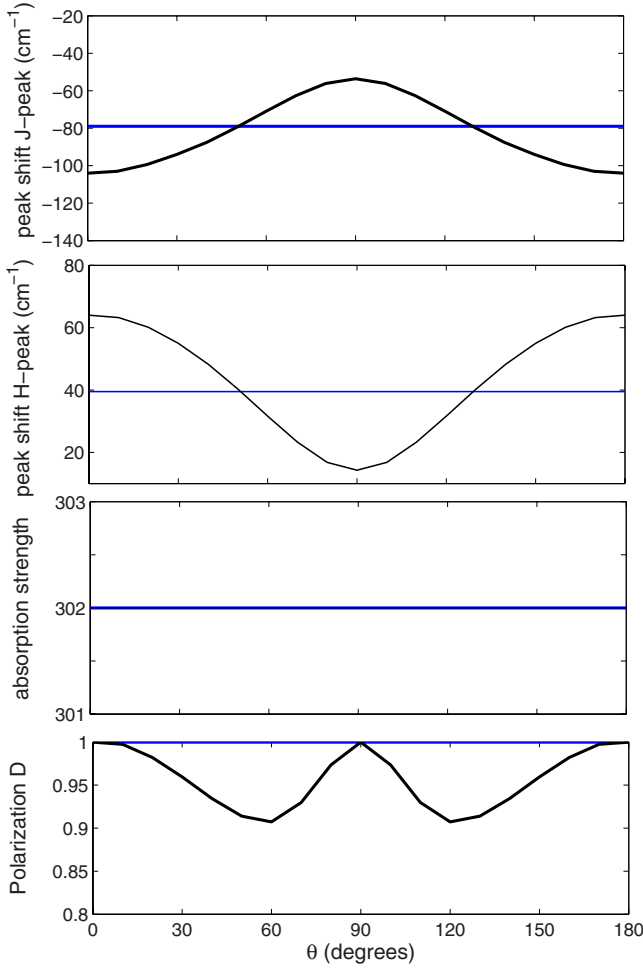
Figure 4. Peak position (upper two graphs), absorption strength (third graph) and polarization (bottom graph) of the two main superradiant peaks as a function of the orientation angle θ. Thick lines: J-transition, thin lines: H-transition. All curves are for equally strong transitions $\mu_x = \mu_y = 8$ D; the blue curve corresponds to degenerate transitions $\omega_x = \omega_y = 0$, while the black curve is an example of non-degenerate transitions, $\omega_y - \omega_x = 50\,\mathrm{cm}^{-1}$. For the first case, there is no orientational dependence (blue lines); in the more general case, the peak positions again vary $\propto \cos(2\theta)$ between the two extremes. In the bottom plot, the polarizations of the J and H transitions are identical.

equal transition dipole moments. In all cases, we use thin lines for the (typically blueshifted) H-transition, and thick lines for the (typically redshifted) J-transition.

The simplest cases occur for angles $\theta = 0°$ or $\theta = 90°$, where the off-diagonal elements of the 2×2-Hamiltonian $H(k)$ all vanish. That is, the optical response is identical the sum of those of two decoupled chains, each of which provides one dominant peak to the absorption spectrum (see appendix A for detailed expressions). For $\theta = 0°$, there is a redshifted absorption peak due to the Q_x-transitions at $E_J^0 = \omega_x - 2\Lambda\mu_x^2$, and a blueshifted absorption peak due to the Q_y-transitions at $E_H^0 = \omega_y + \Lambda\mu_y^2$, where Λ is a positive constant depending on the spatial dependence of the interactions[1]. The absorption strengths are proportional to

---

[1] For nearest neighbour interactions, we have $\Lambda = 1$, while for full dipole–dipole interactions, we have $\Lambda \approx 1.2/a^3$.

respectively ω_x^2 and ω_y^2. At $\theta = 90°$, the role of the two transitions is interchanged: absorption into the Q_y-transitions produces a peak at $E_J^{90} = \omega_y - 2\Lambda\mu_y^2$, while the Q_x-transitions lead to a peak at $E_H^{90} = \omega_x + \Lambda\mu_x^2$, with peak areas proportional to respectively μ_y^2 and μ_x^2. Obviously, in the general case, we may have $\omega_x \neq \omega_y$ and $\mu_x \neq \mu_y$, so that the magnitudes of the shifts and the molecular transition energy that the exciton states are shifted away from (i.e., ω_x or ω_y) are different, leading to different absorption spectra for the two cases $\theta = 0°$ and $\theta = 90°$. Note that, when the transitions Q_x and Q_y are degenerate ($\omega_x = \omega_y$) and equally strong ($\mu_x = \mu_y$), we have $E_J^0 = E_J^{90}$ and $E_H^0 = E_H^{90}$. As is shown in appendix B, we can analytically prove the stronger statement that the absorption spectrum is, in this case, completely independent of θ. Generally, other values of θ lead to exciton states of a mixed Q_x and Q_y-nature. Note that the symmetry of the geometrical arrangement dictates that the results should be symmetric in θ and periodic over $180°$.

In figures 3 and 4, we show the dependence of the transition energies and absorption strengths on the orientation angle θ, for various combinations of transition energies and transition dipole moments. In both plots, the blue lines are for equally strong ($\mu_x = \mu_y = 8$ D) and degenerate ($\omega_x = \omega_y$) transitions. Furthermore, in figure 3, the red and black curves are for degenerate but not equally strong transitions, with red corresponding to $\mu_x = 9$ D and $\mu_y = 7$ D, and black to $\mu_x = 10$ D and $\mu_y = 6$ D. On the other hand, in figure 4, the black curve shows the results for equally strong but non-degenerate transitions, $\omega_y - \omega_x = 50\,\mathrm{cm}^{-1}$. In all cases, thin dashed lines correspond to the blueshifted superradiant transition, and thick lines to the redshifted superradiant transition. Calculations have also been done for the case where the transitions are neither degenerate nor equally strong. Also in this situation, the results are in agreement with the previous analysis and the observable quantities such as peak shifts, absorption strengths and polarizations follow a similar dependence on the orientation angle θ (not shown). For all these parameter combinations, the extrema of the exciton energies and absorption strengths coincide with the two cases $\theta = 0°$ and $\theta = 90°$ discussed above, with the appropriate values for $\omega_x, \omega_y, \mu_x$ and μ_y inserted. For intermediate values of θ, the eigenstates of the superradiant Hamiltonian matrix are of a mixed Q_x and Q_y character and interpolate between these two extremes. Both the energies and absorption strengths have a $\propto \cos(2\theta)$ dependence, consistent with the symmetry and periodicity requirements. It should be noted that the total absorption strength of the two peaks is constant in θ; the mixing only leads to a redistribution of absorption strength over the eigenstates, but the total amount of absorption strength in the doublet is conserved.

Besides the exciton energies and absorption strengths, we also calculate the polarization D, which we quantify by

$$D = \frac{|F_h - F_v|}{F_h + F_v}, \qquad (9)$$

where F_h and F_v are the absorption strengths in the horizontal (x') and vertical (y') direction, respectively. That is, $F_h = |\vec{\mu} \cdot \hat{x}'|^2$ and $F_v = |\vec{\mu} \cdot \hat{y}'|^2$ where $\hat{x}'$ ($\hat{y}'$) is the unit
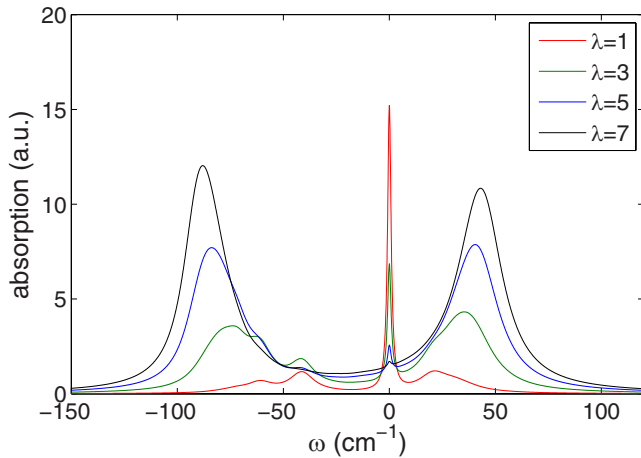
Figure 5. Absorption spectra for various chain length distributions: Poissonian distributions with average lengths $\lambda = 1$ (red), $\lambda = 3$ (green), $\lambda = 5$ (blue), and $\lambda = 7$ (black). All energies are with respect to the monomer transition energy. All chains have the same orientational angle of $\theta = 30°$, and identical monomer transitions with $\mu_x = \mu_y = 8$ D and $\omega_x = \omega_y = \omega_0$; the discussion is equally valid for any other parameter combination. The monomer peak at $\omega = 0\ \mathrm{cm}^{-1}$ is clearly visible, and dimer and trimer peaks around -45 and $-60\ \mathrm{cm}^{-1}$ are identifiable for average lengths $\lambda = 1$ and $\lambda = 3$. The peaks for longer chain lengths become closely spaced and may broaden into one large peak.

vector in the x' (y') direction. This quantity yields $D = 1$ for transitions that are polarized fully horizontally or vertically, while smaller values correspond to deviations from these two extrema. Only in the cases $\theta = 0°$ and $\theta = 90°$ are the eigenstates perfectly polarized in the horizontal (x') and vertical (y') directions; however, figures 3 and 4 show that also in intermediate cases, the eigenstates are still significantly polarized in the horizontal and vertical directions for the J-peak and H-peak, respectively.

As shown in appendix A, the peak positions are length dependent. Since an experimental absorption spectrum will probe chains of different lengths, we also consider a distribution over chain lengths here. The discussion here can be applied to an arbitrary length distribution, which could possibly be extracted from experiment, but we will illustrate the approach for one specific choice of distribution. As a model description, we consider a Poissonian distribution over chain lengths $\tilde{N}$, $P(\tilde{N}) = (\lambda^{\tilde{N}}/\tilde{N}!) \exp(-\lambda)$, where λ is the average chain length [8]. Depending on the details of the distribution over lengths, the bare peak width of a single peak and the separation in energy between peaks for chains of different lengths, such a distribution may either lead to a series of peaks (each peak being a superradiant transition for a specific chain length N) and/or a broadening. The latter occurs when the separation in energy between superradiant peaks of different chain lengths is smaller than or comparable to the peak width.

In figure 5, we show absorption spectra for length distributions of various average width λ. As an example, figure 5 shows the spectra for equally strong and degenerate transitions, but the behaviour discussed here is identical for other parameter choices. The various spectra consist of weighted sums of absorption spectra for a fixed chain

length. It should be noted that, in our formalism, the monomer peak acquires no thermal broadening and is therefore strongly visible in our numerical simulations. This peak is convoluted with a narrow Lorentzian of width $\eta = 1\ \mathrm{cm}^{-1}$ for visualization purposes. For short chain lengths, the peaks for different chain lengths are well separated; for increasingly longer chains, the peak position converges to a fixed value independent of N. As a consequence, length distributions with a short average chain length such as $\lambda = 1$ (red curve in figure 5), we can still distinguish peaks for different chain lengths, in particular $N = 1$ up to $N = 3$. For increasing average chain lengths (e.g., $\lambda = 7$, black curve in figure 5), different lengths lead to closely spaced superradiant peaks, which for this amount of broadening, cannot be resolved separately and lead to a broadened main peak. From an experimental point of view, it might be worthwhile to increase the spectral resolution by decreasing the temperature. Recent experiments [8] have studied fluorescence and fluorescence excitation spectra, where the latter quantity is analogous to the absorption spectrum, for PTCDA complexes on KCl(1 0 0) surfaces, and this has been shown to lead to strongly reduced broadening effects. We anticipate that similar experiments on the porphyrin wires studied here could be sufficiently sensitive to resolve the predicted structure in the absorption spectra.

3.2. Tilted porphyrin chains

Recent studies have shown that it is possible to create non-covalently bound, effectively one-dimensional porphyrin structures on insulating substrates. Meyer and co-workers [30–32] have synthesized chains of tilted porphyrins, both on monolayers and along step edges. In particular, cyanoporphyrins have been shown to form nanowires (among other observed geometries) on a KBr(0 0 1) substrate [30, 31], preferably along the straight step edges. The porphyrins are tilted with respect to the surface and stabilized by electrostatic interactions of the side groups with the surface, with π–π stacking between the porphyrin rings.

The methodology introduced in the present work can also be applied to porphyrin chains where the molecules do not lie flat on the surface. An experimental realization is provided by the cyanoporphyrin systems on KBr(0 0 1) substrates, as studied by the Meyer group [30–32]. Here, the porphyrins form chain-like structures that are stabilized by a combination of electrostatic interactions between the porphyrin side groups and the substrate, and π–π interactions between the porphyrins. The π–π-stacking and the periodicity of the substrate lattice therefore determines the geometry of the structures. We generate a tilted geometry in the way detailed in appendix C. We choose somewhat different parameters in this section as compared to section 3.1, in order to more closely correspond to the experimental situation of [31]. Specifically, the tiled geometry allows for a strongly reduced lattice parameter, which has been reported to be approximately $a = 0.6$ nm [31]. Also, given the asymmetry of the porphyrin and the reported estimated transition dipole moment [30] of $\mu = 4.4$ D, we choose reduced and unequal transition dipole moments with respect to section 3.1, $\mu_x = 4.4$ D and
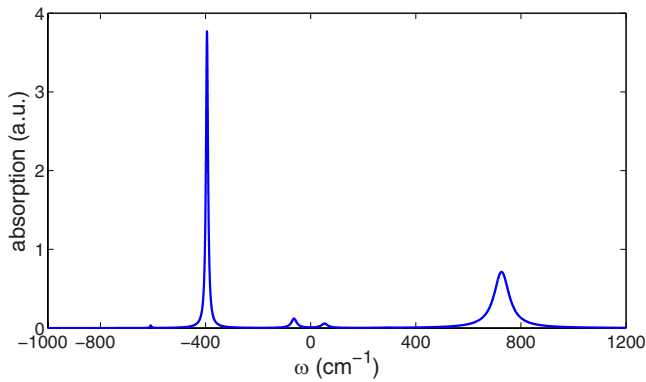
Figure 6. Absorption peak positions for a tilted porphyrin chain of length $N = 5$, with geometrical parameters $\theta = 30°$, $\alpha = 40°$, $\beta = -40°$. The two main peaks have a similar area, despite their large difference in broadening. The small peaks in the centre of the plot are higher order contributions, i.e. the $k = 3$ states of appendix A.

$\mu_y = 3$ D. For clarity, we choose equal transition energies and will not show results for other parameter sets, but it should be noted that the generic double-peaked structure of the absorption spectrum remains the same.

Due to the close proximity of the molecules, it is more accurate to use extended dipole interactions [51], where instead of point dipoles, we consider the Coulomb interactions between two spatially separated positive and negative charges. The value of the point charges and their separation should be chosen such that the correct transition dipole moment vector is reproduced. This leaves the charge separation distance as the single free parameter, which in these simulations, we take as $L = 0.6$ nm [24]. Note that the spectra presented here are only meant as qualitative predictions; the precise magnitude of the energy shifts depends strongly on the precise relative orientation of and distance between the molecules. As a consistency check, it should be noted that the shifts we obtain for Soret band transitions are typically of the order of a few thousand cm^{-1}, which is of a similar order of magnitude as the shifts that have been observed in cylindrical porphyrin aggregates, where the porphyrin molecules are similarly closely stacked [20–22, 24].

In figure 6, we show the absorption peak positions for the geometrical parameters $\theta = 30°$, $\alpha = 40°$, $\beta = -40°$, as a typical example. As can be seen in figure 6, the qualitative behaviour in the case of tilted porphyrins is quite similar to the flat-lying porphyrin structures; again, the absorption is dominated by two peaks of comparable area, where one tends to be redshifted while the other is blueshifted with respect to the monomer transition. However, the tilted orientation allows for a much closer packing of the porphyrins, and correspondingly much stronger interactions and larger shifts. In this case, the thermal energy $kT = 200$ cm^{-1} is smaller than or at most comparable to the energy spacing of the various exciton levels. This implies that the J-peak dephases only very slowly due to a lack of relaxation channels, leading to a narrow absorption peak. In contrast, the H-peak has an abundance of relaxation pathways into lower lying exciton states, implying a short lifetime and a correspondingly strong

broadening, as is confirmed in figure 6. Note, however, that despite their strongly different linewidths, the areas of these two peaks are of comparable magnitude. In tilted porphyrin chains, the transition dipole moments will in general also have an out-of-plane component. However, there is still a tendency for the superradiant blueshifted state to be polarized mostly perpendicular to the x'-axis, and for the superradiant redshifted state to be polarized mostly parallel to the x'-axis. Generally, the increased number of orientational degrees of freedom prohibits a simple analysis of the precise magnitude of the shifts, as was possible in the planar case discussed in section 3.1.

Also in the case of tilted porphyrin chains, a distribution over chain lengths will occur in practice. This leads to a total absorption that is a weighted sum of absorption contributions for fixed length N, where longer chain lengths lead to larger peak shifts and with the peak shifts eventually converging to the long chain length limit; this is completely analogous to the situation for planar porphyrin structures. The main difference lies in the magnitude of the peak shifts, which tends to be on the order of several hundreds of cm^{-1} for these close-packed tilted porphyrin structures, and up to several thousands of cm^{-1} for Soret band transitions, as compared to the shifts of tens to at most hundreds of cm^{-1} for the planar porphyrin chains. This leads to superradiant peaks for different chain lengths N that are far more clearly separated as compared to the planar geometry, and this suggests that a tilted porphyrin arrangement provides an experimentally more straightforward test of the predictions given here. Depending on the homogeneous and thermal broadening of the individual peaks, the main peaks for different chain lengths may be spectrally resolved if the separation between peaks is at least of a similar size as the peak widths. This suggests that such a series of peaks is most likely to be visible in the low energy range of the spectrum, where the narrow J-peaks reside. Likewise, as mentioned in section 3.1, low temperature experiments analogous to those by Müller *et al* [8] are expected to lead to strongly reduced broadening and a corresponding increase in the spectral resolution.

4. Conclusions

We have shown that a number of porphyrin structures on surfaces that have recently been experimentally realized should exhibit interesting collective optical properties. In particular, the coupling between the transition dipole moments of the porphyrin molecules leads to collective electronic excitations, which spectroscopically will be manifested through superradiant effects in both the Soret band and the Q-band. Generally, for a fixed chain length, the absorption spectrum in either band will be dominated by two such superradiant peaks where one will be redshifted and the other will be blueshifted with respect to the monomer transition energy. Their energies, polarizations and absorption strengths can be understood in terms of Davydov splitting between the superradiant transitions resulting from the Q_x and Q_y transitions.

For porphyrin structures where the porphyrins lie flat on the surface, inter-porphyrin distances are relatively large,

resulting in couplings and peak shifts of the order of tens to a few hundred cm^{-1}. If the Q_x and Q_y transitions are equally strong and degenerate, the absorption spectrum is shown to be independent of the relative orientation of the porphyrins. This orientational invariance is broken if the transitions are not degenerate or have different transition dipole moments. In that case, the energies and absorption strengths depend sinusoidally on the orientation angle. Tilted porphyrins lead to a qualitatively similar picture; however, these systems allow for a much closer spacing of the porphyrins, so that the interporphyrin couplings and resulting absorption peak shifts are considerably larger, already reaching hundreds of cm^{-1} for the relatively weak Q-band transitions and which can be of the order of thousands of cm^{-1} for Soret band transitions. The two-peaked structure of the absorption spectrum for a given chain length is also observed here. The considerably larger interporphyrin interactions and resultant shifts suggest that tilted porphyrin geometries, rather than flat porphyrin geometries, provide a better experimental test of the absorption spectra predicted here.

Experimentally, there will be a distribution over chain lengths. Such a distribution will lead to a series of peaks in the absorption spectrum, where each peak corresponds to the superradiant transition for a given chain length. If the peaks are sufficiently closely spaced with respect to their widths, the spread in chain length leads to a broadening of the excitonic peak. We anticipate that low-temperature experiments, analogous to those performed in [8] for PTCDA molecules on KCl(1 0 0) substrates, give a considerable increase in spectral resolution and could thereby probe the predicted absorption peak structure.

Appendix A. Expressions for non-disordered chains

In the absence of disorder, we have $\omega_{nj} = \omega_j$. We do allow for different transition energies and different transition dipole moments for each transition. In that case, the Hamiltonian reads

$$H = \sum_{nj} \omega_j \left| n; j \right\rangle \left\langle n; j \right| + \sum_{njn'j'} J_{jj'} (n - m) \left| n; j \right\rangle \left\langle m; j' \right|.$$
(A1)

The interactions $J_{jj'}(n - m)$ are taken as dipole–dipole interactions between transition j on molecule n, and transition j' on molecule $m \neq n$. The point dipole–dipole interaction between two transition dipole moments $\vec{\mu}_{mj}$ and $\vec{\mu}_{nj'}$, located at positions $\vec{r}_m$ and $\vec{r}_n$ respectively, is given by the well-known expression

$$J_{jj'} (n - m) = \frac{\vec{\mu}_{mj} \cdot \vec{\mu}_{nj'}}{r^3} - 3 \frac{(\vec{\mu}_{mj} \cdot \vec{r}_{nm}) (\vec{\mu}_{nj'} \cdot \vec{r}_{nm})}{r^5},$$
(A2)

where we have defined $\vec{r}_{nm} = \vec{r}_n - \vec{r}_m$ and $r = |\vec{r}_{nm}|$. Then, the interactions $J_{jj'}(n - m)$ for the various combinations of j and j' all have the same distance dependence, so that the various sub-Hamiltonians $H_{jj'}$ are diagonalized by the same transform. Moreover, this transform is the transform $|k\rangle = \sum_n c_{kn} |n\rangle$ that diagonalizes the chain with one transition per molecule;

application of this transformation leads to a set of $j \times j$-matrices $H(k)$ that remain to be diagonalized.

The exciton chain with one transition per molecule provides a useful reference case, from which we can understand the more general case of multiple transitions per molecule, as discussed in the main text of this paper. The remainder of appendix A, and specifically equations (A3)–(A5), concern results and discussion for a chain with one transition per molecule. In this case, the absorption is dominated by one superradiant transition, where all the molecules absorb in phase. For a chain with one transition per molecule and with nearest-neighbour interactions J, $H = \sum_n \omega_0 |n\rangle \langle n| + J \sum_n (|n\rangle \langle n + 1| + |n + 1\rangle \langle n|)$, we can solve explicitly for the wave functions, energies, absorption strengths and so forth. The wave function for exciton state k is

$$c_{kn} = \sqrt{\frac{2}{N + 1}} \sin \left(\frac{\pi k n}{N + 1} \right),$$
(A3)

with energy

$$E_k = \omega_0 + 2J \cos \left(\frac{\pi k}{N + 1} \right),$$
(A4)

and absorption strength

$$O_k = \frac{1 - (-1)^k}{N + 1} \cot^2 \frac{\pi k}{2 (N + 1)}.$$
(A5)

It is easily seen that the $k = 1$ state contains the bulk of the absorption strength, while the remainder is shared by the other odd states. Corrections can be obtained for including interactions beyond the nearest neighbour, leading to some additional shifts, but the qualitative discussion is identical [52, 53].

The sign of the interaction, and thus also the energy of the superradiant state, depend on the orientation of the molecular transition dipole moment with respect to the vector connecting the molecules in the chain, where θ is the angle between the two. This directly results from substituting the molecular transition dipole moments $\vec{\mu}$ into the dipole–dipole interaction expression, equation (A2). The interactions are negative for $\theta < 54.7°$, which are referred to as J-aggregates and where the superradiant peak is lower in energy than the monomer peak, and the interactions are positive for $\theta > 54.7°$, the H-aggregates with a superradiant absorption peak with a blueshifted energy. Note that for $\theta = 0°$, the magnitude of the interactions is twice as large as for the case of $\theta = 90°$ (see equation (A2)), besides differing in sign. In addition, it should be noted that the energies and absorption strengths are length dependent.

Appendix B. Orientational invariance for flat-lying porphyrin chains

For a chain of in-plane porphyrins, we have $\vec{\mu}_{n,(j=x)} = \vec{\mu}_x = \mu_x(\cos\theta, \sin\theta, 0)$ and $\vec{\mu}_{m,(j=y)} = \vec{\mu}_y = \mu_y(\sin\theta, -\cos\theta, 0)$.

We can then write out the various forms that $J_{jj'}(n-m)$ can take (again, a is the lattice constant):

$$\frac{J_{xx}(n-m)}{\mu_x^2} = \frac{1 - 3\cos^2\theta}{|n-m|^3 a^3} \tag{B1}$$

$$\frac{J_{yy}(n-m)}{\mu_y^2} = \frac{1 - 3\sin^2\theta}{|n-m|^3 a^3} \tag{B2}$$

$$\frac{J_{xy}(n-m)}{\mu_x\mu_y} = \frac{J_{yx}(n-m)}{\mu_x\mu_y} = \frac{-3\cos\theta\sin\theta}{|n-m|^3 a^3}. \tag{B3}$$

As mentioned before, application of the transformation $|k\rangle = \sum_n c_{kn}|n\rangle$ to equation (A1) partially diagonalizes the Hamiltonian. For each value of k, this leads to the Hamiltonian matrix

$$H(k) = \begin{pmatrix} \omega_x & 0 \\ 0 & \omega_y \end{pmatrix} + \frac{f(k)}{a^3}$$
$$\times \begin{pmatrix} \mu_x^2(1 - 3\cos^2\theta) & -3\mu_x\mu_y\cos\theta\sin\theta \\ -3\mu_x\mu_y\cos\theta\sin\theta & \mu_y^2(1 - 3\sin^2\theta) \end{pmatrix}. \tag{B4}$$

In the case of degenerate and equally strong transitions Q_x and Q_y, that is, $\omega_x = \omega_y \equiv \omega_0$ and $\mu_x = \mu_y \equiv \mu$, this result simplifies greatly. Labeling the two eigenstates by $s = \pm$, the eigenenergies are

$$E_{ks} = \omega_0 + \frac{f(k)\mu^2}{2a^3}(-1 \pm 3). \tag{B5}$$

Note that the eigenenergies are independent of the orientations of the porphyrins. The normalized eigenvectors are given by

$$\vec{d}_+ = (-\sin\theta, \cos\theta), \tag{B6}$$

$$\vec{d}_- = (\cos\theta, \sin\theta). \tag{B7}$$

The corresponding transition dipole moments are easily found by filling in equation (8), and are seen to be independent of the orientation angle θ as well,

$$\vec{\mu}_{k+} = \left(\sum_n c_{kn}\right)\left[\mu\cos\theta\begin{pmatrix}\cos\theta\\\sin\theta\\0\end{pmatrix} + \mu\sin\theta\begin{pmatrix}\sin\theta\\-\cos\theta\\0\end{pmatrix}\right]$$
$$= \mu\left(\sum_n c_{kn}\right)\begin{pmatrix}1\\0\\0\end{pmatrix}, \tag{B8}$$

$$\vec{\mu}_{k-} = \left(\sum_n c_{kn}\right)\left[-\mu\sin\theta\begin{pmatrix}\cos\theta\\\sin\theta\\0\end{pmatrix} + \mu\cos\theta\begin{pmatrix}\sin\theta\\-\cos\theta\\0\end{pmatrix}\right]$$
$$= \mu\left(\sum_n c_{kn}\right)\begin{pmatrix}0\\-1\\0\end{pmatrix}. \tag{B9}$$

In other words, the entire absorption spectrum is independent of the orientation of the porphyrins.

Appendix C. Geometry for tilted porphyrin chains

To generate a chain of tilted porphyrin molecules, we start out from flat-lying porphyrin molecules, so that the transition dipole moments of the two transitions are $\vec{\mu}_x = \mu_x(\cos\theta, \sin\theta, 0)$ and $\vec{\mu}_y = \mu_y(\sin\theta, -\cos\theta, 0)$. We generate a tilted geometry by applying two additional (internal) rotations to the molecules. First, we rotate around the x'-axis over an angle α. Subsequently, we rotate around the new rotated y'-axis over an angle β. We employ the convention that positive signs correspond to counterclockwise rotations when looking towards the origin, and both angles are allowed to have both positive and negative values. This corresponds to applying the rotation matrix

$$A = \begin{pmatrix} \cos\beta & 0 & \sin\beta \\ \sin\alpha\sin\beta & \cos\alpha & -\sin\alpha\cos\beta \\ -\cos\alpha\sin\beta & \sin\alpha & \cos\alpha\cos\beta \end{pmatrix} \tag{C1}$$

to the transition dipole vectors. A subsequent calculation of the interactions, through point-dipole interactions, extended dipole interactions or some other method of choice, then fully defines the Hamiltonian.

Appendix D. Thermal line broadening

We use the formalism developed in [47] to obtain a lineshape for the excitonic transitions. That is, we allow for a coupling of the excitons with acoustic phonons in the environment, which we treat as a perturbation. From Fermi's golden rule, we obtain phonon-induced scattering rates from exciton state s to exciton state r,

$$W_{rs} = W_0 S(|\omega_r - \omega_s|) G(\omega_r - \omega_s) \sum_n c_{sn}^2 c_{rn}^2, \tag{D1}$$

i.e. the product of an overall amplitude W_0, a one-phonon spectral density $S(\omega)$, a thermal occupation factor $G(\omega)$, and an overlap factor between the initial and final state. The thermal occupation factor is given by $G(\omega) = n(\omega)$ for $\omega > 0$, and by $G(\omega) = 1 + n(-\omega)$ for $\omega < 0$, with $n(\omega) = (\exp(\omega/k_B T) - 1)^{-1}$ being the thermal occupation of a phonon mode of energy ω. The relaxation channels that are included in this way lead to a dephasing of the exciton states, and the dephasing rate of exciton state s is simply given by $\Gamma_s = \frac{1}{2}\sum_r W_{rs}$.

References

[1] Lehn J-M 1988 *Angew. Chem. Int. Edn* **27** 89
[2] Whitesides G M, Mathias J P and Seto C T 1991 *Science* **254** 1312
[3] Whitesides G M and Grzybowski B 2002 *Science* **295** 2418
[4] Shelnutt J A and Medforth C J 2013 Self-assembled porphyrin nanostructures, their potential applications *Organic Nanomaterials: Synthesis, Characterization, Device Applications* ed T Torres and G Bottari (New York: John Wiley)
[5] Yokoyama T, Yokoyama S, Kamikado T, Okuno Y and Mashiko S 2001 *Nature* **413** 619
[6] Barth J V, Costantini G and Kern K 2005 *Nature* **437** 671

J. Phys. D: Appl. Phys. **47** (2014) 305301

S M Vlaming and A Eisfeld

[7] Repp J, Meyer G, Paavilainen S, Olsson F E and Persson M 2006 *Science* **312** 1196

[8] Müller M, Paulheim A, Eisfeld A and Sokolowski M 2013 *J. Chem. Phys.* **139** 044302

[9] Fidder H, Knoester J and Wiersma D A 1990 *Chem. Phys. Lett.* **171** 529

[10] Kobayashi T (ed) 1996 *J-Aggregates* (Singapore: World Scientific)

[11] Scheibe G 1966 *Optische Anregungen organischer Systeme* ed W Foerst (Weinheim: Verlag Chemie) p 109 and references therein

[12] Lever A B P (ed) 1983 *Iron Porphyrins* (Reading, MA: Addison-Wesley)

[13] Gouterman M, Rentzepis P M and Straub K D (ed) 1986 *Porphyrins: Exicted States and Dynamics* (Washington, DC: American Chemical Society)

[14] Scheer H 1991 *Chlorophylls* (Boca Raton, FL: CRC Press)

[15] Hosomizu K, Oodoi M, Umeyama T, Matano Y, Yoshida K, Isoda S, Isosomppi M, Tkachenko N V, Lemmetyinen H and Imahori H 2008 *J. Phys. Chem. B* **112** 16517

[16] Cho H S, Jeong D H, Cho S, Kim D, Matsuzaki Y, Tanaka K, Tsuda A and Osuka A 2002 *J. Am. Chem. Soc.* **124** 14642

[17] Wagner R W and Lindsey J S 1994 *J. Am. Chem. Soc.* **116** 9759
Ambroise A, Kirmaier C, Wagner R W, Loewe R S, Bocian D F, Holten D and Lindsey J S 2002 *J. Org. Chem.* **67** 3811

[18] Kim Y H, Jeong D H, Kim D J, Sae Chae, Cho H S, Keun K S, Aratani N and Osuka A 2001 *J. Am. Chem. Soc.* **123** 76

[19] Hernando J, de Witte P A J, van Dijk E M H P, Korterik J, Nolte R J M, Rowan A E, Garcia M F and van Hulst N F 2004 *Angew. Chem.* **116** 4137
Hernando J, de Witte P A J, van Dijk E M H P, Korterik J, Nolte R J M, Rowan A E, Garcia M F and van Hulst N F 2004 *Angew. Chem. Int. Edn* **43** 4045

[20] Gandini S C M, Gelamo E L, Itri R and Tabak M 2003 *Biophys. J.* **85** 1259

[21] Rotomskis R, Augulis R, Snitka V, Valiokas R and Liedberg B 2004 *J. Phys. Chem. B* **108** 2833

[22] Doan S C, Shanmugham S, Aston D E and McHale J L 2005 *J. Am. Chem. Soc.* **127** 5885

[23] Akins D L, Zhu H-R and Guo C 1994 *J. Phys. Chem.* **98** 3612
Akins D L, Zhu H-R and Guo C 1996 *J. Phys. Chem.* **100** 5420

[24] Vlaming S M, Augulis R, Stuart M C A, Knoester J and van Loosdrecht P H M 2009 *J. Phys. Chem. B* **113** 2273

[25] Hill J P, Xie Y, Akada M, Wakayama Y, Shrestha L K, Ji Q and Ariga K 2013 *Langmuir* **29** 7291

[26] Haq S, Hanke F, Dyer M S, Persson M, Iavicoli P, Amabilino D B and Raval R 2011 *J. Am. Chem. Soc.* **133** 12031

[27] Otsuki J, Nagamine E, Kondo T, Iwasaki K, Asakawa M and Miyake K 2005 *J. Am. Chem. Soc.* **127** 10400

[28] Wang Y, Wu K, Kröger J and Berndt R 2012 *AIP Adv.* **2** 041402

[29] Papageorgiou N, Salomon E, Angot T, Layet J M, Giovannelli L and Lay G L 2004 *Prog. Surf. Sci.* **77** 139

[30] Zimmerli L, Maier S, Glatzel Th, Gnecco E, Pfeiffer O, Diederich F, Fendt L and Meyer E 2007 *J. Phys.: Conf. Ser.* **61** 1357

[31] Maier S, Fendt L, Zimmerli L, Glatzel Th, Pfeiffer O, Diederich F and Meyer E 2008 *Small* **4** 1115

[32] Glatzel Th, Zimmerli L and Meyer E 2008 *Isr. J. Chem.* **48** 107

[33] Tröppner C, Schmitt T, Reuschl M, Hammer L, Schneider M A, Mittendorfer F, Redinger J, Podloucky R and Weinert M 2012 *Phys. Rev. B* **86** 235407

[34] Schmitt T and Schneider M A unpublished results

[35] Zhou Y, Wang B, Zhu M and Hou J G 2005 *Chem. Phys. Lett.* **403** 140

[36] Glatzel Th, Zimmerli L, Kawai S, Meyer E, Fendt L and Diederich F 2011 *Beilstein J. Nanotechnol.* **2** 34

[37] Tretiak S, Chernyak V and Mukamel S 1998 *Chem. Phys. Lett.* **297** 357

[38] Anderson H L, Martin S J and Bradley D D C 1994 *Angew. Chem. Int. Edn Engl.* **33** 655

[39] Schalk O, Brands H, Balaban T S and Unterreiner A-N 2008 *J. Phys. Chem. A* **112** 1719

[40] Arai Y and Segawa H 2010 *Chem. Commun.* **46** 4279

[41] Zimmermann J, Siggel U, Fuhrhop J-H and Röder B 2003 *J. Phys. Chem. B* **107** 6019

[42] Yildirim H, Işeri E I and Gülen D 2004 *Chem. Phys. Lett.* **391** 302

[43] Gülen D 2006 *Photosynthesis Res.* **87** 205

[44] Stradomska A and Knoester J 2010 *J. Chem. Phys.* **133** 094701

[45] Davydov A S 1971 *Theory of Molecular Excitons* (New York: Plenum)

[46] Agranovich V M and Galanin M D 1982 *Electronic Excitation Energy Transfer in Condensed Matter* ed V M Agranovich and A A Maradudin (Amsterdam: North Holland)

[47] Heijs D J, Malyshev V A and Knoester J 2005 *Phys. Rev. Lett.* **95** 177402
Heijs D J, Malyshev V A and Knoester J 2005 *J. Chem. Phys.* **123** 144507

[48] Anderson P W 1958 *Phys. Rev.* **109** 1492

[49] Abrahams E, Anderson P W, Licciardello D C and Ramakrishnan T V 1979 *Phys. Rev. Lett.* **42** 673

[50] Möbius S, Vlaming S M, Malyshev V A, Knoester J and Eisfeld A One-dimensional excitonic systems with diagonal Lévy disorder: a detailed study of the absorption spectra and the disorder scaling of localization length *submitted*

[51] Didraga C, Pugžlys A, Hania P R, von Berlepsch H, Duppen K and Knoester J 2004 *J. Phys. Chem. B* **108** 14976

[52] Fidder H, Knoester J and Wiersma D A 1991 *J. Chem. Phys.* **95** 7880

[53] Malyshev V and Moreno P 1995 *Phys. Rev. B* **51** 14587